Clays and Clay Minerals, Vol. 45, No. 1, 77–84, 1997.

INTERCALATION CHARACTERISTICS OF RHODAMINE 6G IN FLUOR-TAENIOLITE: ORIENTATION IN THE GALLERY

TAKETOSHI FUJITA,[1] NOBUO IYI,[1] TETSUSHI KOSUGI,[2]
AKITSUGU ANDO,[2] TAKAHIRO DEGUCHI[3] AND TAKAYUKI SOTA[3]

[1]National Institute for Research in Inorganic Materials, Namiki 1-1, Tsukuba, Ibaraki, 305 Japan

[2]Topy Industries Limited, Akemi-cho 1, Toyohashi, Aichi, 440 Japan

[3]Department of Electrical Engineering, Waseda University, Shinjuku, Tokyo, 169 Japan

Abstract—The orientation of rhodamine 6G (R6G) in the 22-Å basal-spaced complex with Li-fluor-taeniolite has been studied using X-ray powder diffraction, 1-dimensional Fourier analysis, polarized infrared (IR) spectroscopy, carbon analysis and thermal analysis. The R6G was adsorbed by cation exchange in aqueous solution. In the range of 0.086 to 0.46 molar ratio of R6G to taeniolite, the basal spacings of the complex were nearly constant at 21.7 to 22.2 Å. From X-ray diffraction (XRD) data, it was confirmed that R6G in the complex orients with its longest xanthene ring axis perpendicular to the *ab* plane of the host. The pleochroism of IR absorption bands at 1331, 1517, 1537 and 1621 cm^{-1} supports the vertical orientation. The wide stability range of the vertical configuration is consistent with the strong coulombic force between the highly negatively charged silicate layer of the host [cation exchange capacity (CEC) = 157 ± 9 meq/100 g] and the positively charged nitrogen bonded to both sides of the R6G xanthene ring.

Key Words—Infrared Spectroscopy, Intercalation, Li-fluor-Taeniolite, Mica, Rhodamine 6G, X-ray Diffraction.

INTRODUCTION

Smectites and related compounds intercalate various kinds of molecules and ions into their 2-dimensional gallery. Complexes of organic compounds with phyllosilicate are known to form so-called "nanocomposites" (Fukushima and Inagaki 1987; Wu and Lerner 1993; Wang and Pinnavaia 1994). Among them, the nylon-montmorillonite complex shows excellent mechanical properties and higher thermal resistivity, which are never realized by individual compounds (Okada et al. 1990).

There are many studies of the intercalation of organic dyes into phyllosilicates, focusing on such topics as: 1) assessment of the host surface by spectrum change of the adsorbed dye molecule (Cenens et al. 1987); 2) photocatalytic reaction in colloidal clay systems (DellaGuardla and Thomas 1983); 3) stabilization of photolabile pesticide on the clay with a co-adsorption of organic cation as an energy acceptor (Margulies et al. 1985); and 4) photochemical reduction of water to obtain H_2 and O_2 with the aid of a catalyst (Villemure et al. 1986; Nijs et al. 1983).

R6G, a typical xanthene dye whose composition is expressed as $(C_{28}H_{31}N_2O_3)^+ Cl^-$, is known as a laser dye. One of its most serious limitations as a laser dye is its low heat resistivity. An increase in the thermal resistance of coumarin dye intercalated to montmorillonite has been reported (Endo et al. 1989). Similar stabilization may be expected in the R6G complex with phyllosilicates. Several studies have been performed of the intercalation of R6G into phyllosilicates to examine the spectroscopic properties of the intercalated state; however, its configuration in the interlayer space remains unclear (Endo et al. 1986, 1988; Tapia Estevez et al. 1994). R6G complexes reported thus far take a different basal distance, depending on the concentration of the dye (Lopez Arbeloa et al. 1982). In the course of our study of the intercalation of R6G to taeniolite, we found a wide stability range for the 22-Å basal distance in R6G-taeniolite, which directly changed from the 12.3-Å spacing of taeniolite without R6G in its gallery. This differs from the former reports, in which the 20–21-Å phase has a narrow stability range, and changes gradually to narrower basal spacings according to composition.

The purpose of this study is to clarify the configuration of R6G in the gallery of phyllosilicate.

EXPERIMENTAL

Materials

The host material, Li-taeniolite (LiTN: $LiMg_2LiSi_4O_{10}F_2$) was prepared as follows. The Na^+ ions of synthetic Na fluor-taeniolite ($NaMg_2LiSi_4O_{10}F_2$, Topy Industries) were exchanged with Li by reaction at 80 °C with an excess amount of LiCl aqueous solution for 2 h. Excess of chloride ions was removed by repeated washing. Then the 0.3-μm median particle size fraction was separated by sedimentation. A suspension of the fraction was pipetted onto a glass plate to form a thin film, used as a host. The CEC of the host material was determined to be 157 ± 9 meq/100 g by the ammonium acetate adsorption method (Schol-

Copyright © 1997, The Clay Minerals Society

https://doi.org/10.1346/CCMN.1997.0450109 Published online by Cambridge University Press

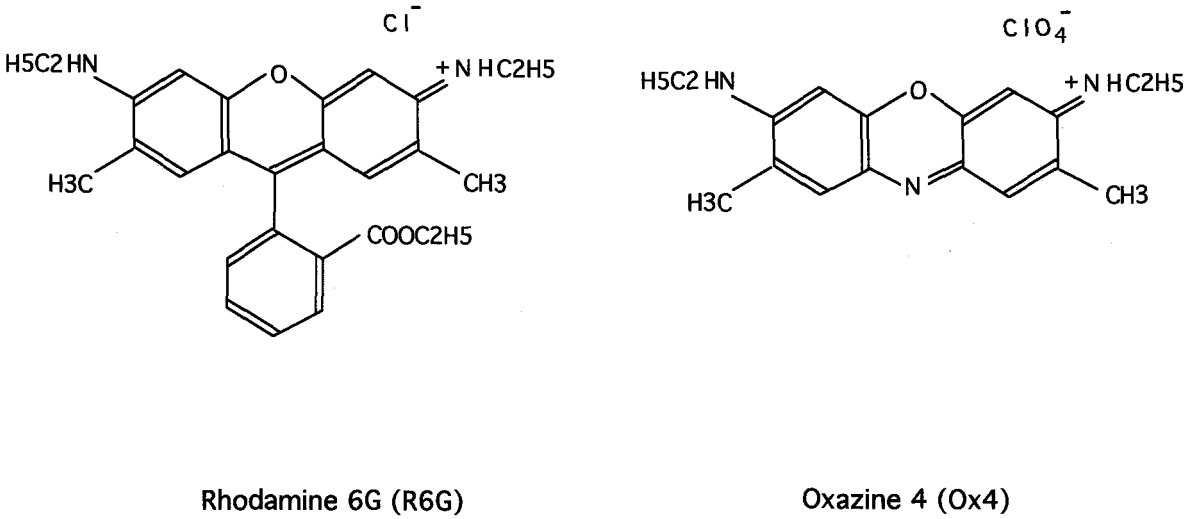

Figure 1. The chemical formulae of rhodamine 6G and oxazine 4.

lenberger and Simon 1946). Laser grade R6G and oxazine 4 (Lambda Physik) were used as the guests without further purification. An oxazine 4 (Ox4) complex was also synthesized to check the results of R6G, because its molecular structure is similar to that of R6G (Figure 1). Four substituents on both sides of the phenoxazine frame are the same as those of R6G. The length of the longest molecular axis is the same, as is the positive charge of the 2 N atoms. Thus, its intercalation configuration may help to characterize the intercalation behavior of R6G.

Intercalation of R6G to LiTN

The LiTN-dye complexes were prepared by immersing the LiTN film in R6G aqueous solution. Intercalation of R6G was attained by a cation exchange reaction between Li^+ in the TN layer and the R6G cation (= R6G without Cl^-). The reaction was performed using a decomposition vessel under autogene pressure of reaction temperature, and a rapid-quench type hydrothermal apparatus operating at 100 MPa (Yamada et al. 1988). The exchange temperature was changed from 200 to 80 °C, and the duration was set at 48 h. A similar procedure was applied for the preparation of the Ox4 complex.

Characterization of R6G-TN complex

The XRD intensities were measured at 30 °C under a controlled relative humidity of 20% by a powder diffractometer, RINT 2000 (Rigaku), using monochromatized Cu$K\alpha$ radiation.

An IR absorption spectrum was obtained using a Perkin-Elmer Model 1600 FT-IR spectrometer with a linearly polarized incident beam. As shown in Figure 2, a film of R6G-TN complex was placed on the plane with a fixed angle of 30° with respect to the incident beam, and 60° to the polarization plane. The direction of polarization was rotated from $\theta = 0°$ to 90° in the polarization plane perpendicular to the beam direction, to detect the pleochroism of the spectrum. At $\theta = 0°$, the incident beam resolved into 2 components parallel and perpendicular to the specimen plane, which preferentially oriented parallel to the holder plane, at an angle of 30° to the incident beam. At $\theta = 90°$, only vibrational modes parallel to the silicate plane are activated. If a heterocyclic ring of R6G or Ox4 is perpendicular to the host layer, the IR active vibrational mode that is parallel to the heterocyclic ring plane should show maximum interaction with the beam with its polarization angle of $\theta = 0°$, and minimum at $\theta = 90°$. However, there should be almost no θ angle dependency for parallel arrangement of the heterocyclic ring of the guest molecules to the host layer.

Thermogravimetry (TG) and differential thermal analysis (DTA) were performed using a TAS-200 thermal analyzer (Rigaku). Approximately 5 to 8 mg of specimen were heated at the rate of 10 °C/min from room temperature to 1000 °C in air using Al_2O_3 powder as a reference material. The R6G content was determined by carbon analyses, as measured by an RW-12 automatic carbon analyzer (LECO, United States). Weight loss at 1000 °C was used to check the carbon analysis data.

Refinement

The integrated intensities of 00*l* reflections up to $l = 10$ were used for 1-dimensional Fourier analysis as well as least-squares refinement. The composition of the specimen was TN:R6G:H_2O = 1:0.45:2.6 in molar ratio. The observed intensities were corrected for random powder Lorentz-polarization factor. The starting parameters of the mica portion of the structure for the least-squares and Fourier synthesis were taken from the refined parameters for K-TN obtained by the single

https://doi.org/10.1346/CCMN.1997.0450109 Published online by Cambridge University Press

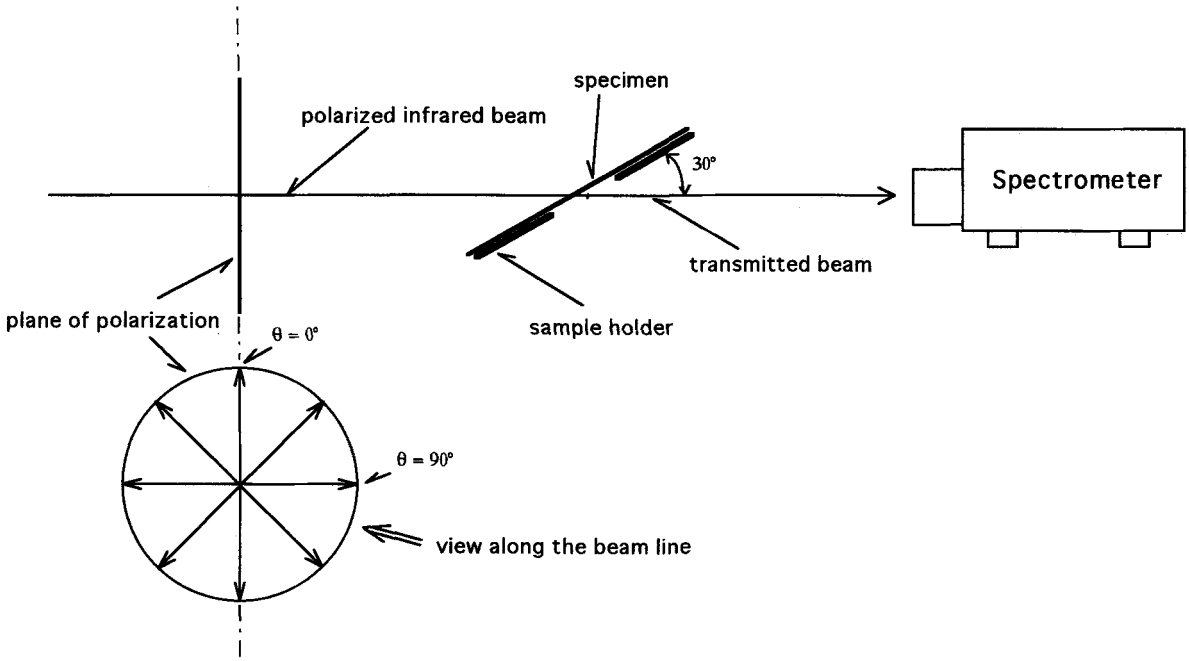

Figure 2. The scheme of polarized IR absorption measurement.

crystal XRD method (Toraya et al. 1977). Their work also provided the grounds for assuming a centrosymmetrical structure for the R6G-TN complex. The positions of the atoms in the R6G molecule portion of the structure were calculated on the basis of ideal organic C-C bond length data. Neutral atom scattering factors were taken from Ibers and Hamilton (1974), and hydrogens were incorporated onto the attached C or N atoms. The remaining Li in the gallery was ignored in the calculation because of its low scattering factor. The least-squares refinements were performed assuming 2 types of models:

1) The longest axis of the R6G xanthene ring is perpendicular to the silicate layer ("vertical model") as shown in Figure 3. The statistical distribution of the 2 possible directions of the ethoxy carbonyl group, which is bonded to the ortho position of the phenyl group in R6G, is expressed as 2 "½" ethoxy carbonyl groups in the figure. In the refinement, the occupancy of the R6G molecule in the gallery was varied as well as the rotation angle of the phenyl group and position of the ethoxy carbonyl group.

2) The plane of the xanthene ring is parallel to the *ab* plane of the host in 3 layers: 2 non-center R6G

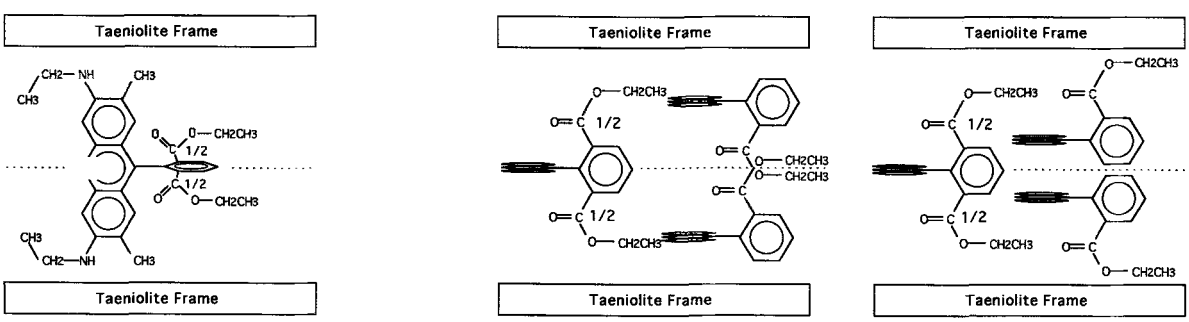

(a) Type I (b) Type II

Vertical model **Parallel model**

Figure 3. The intercalation model for the Fourier analyses. The notation "½" indicates the statistical distribution of 2 possible directions of the ethoxy carbonyl group.

https://doi.org/10.1346/CCMN.1997.0450109 Published online by Cambridge University Press

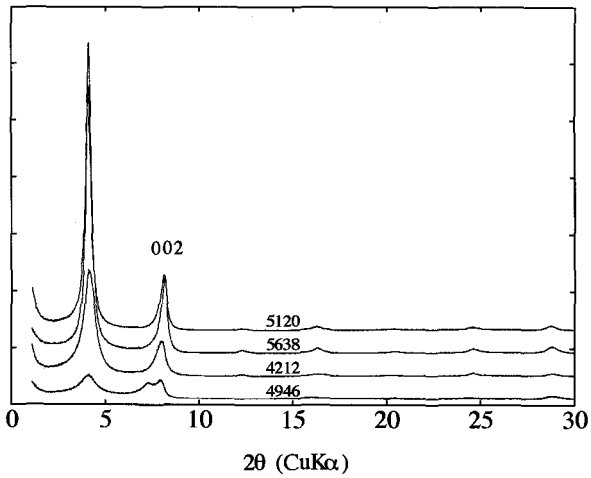

Figure 4. The XRD patterns of rhodamine 6G-taeniolite with the variation of rhodamine 6G content of the composite.

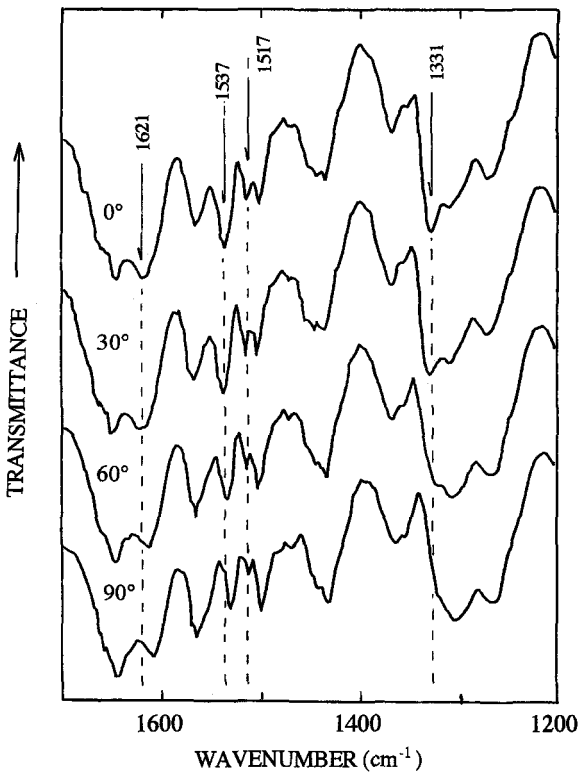

Figure 5. The change in FTIR spectra of rhodamine 6G-taeniolite with variation of polarization angle of incident beam (θ).

layers and 1 R6G layer in the center of the gallery ("parallel model"), as shown in Figure 3. Two types of directions for the non-center R6G molecule were considered: one in which the ethoxy carbonyl group is pointing inward to the center of the gallery (type I), and the other in which the ethoxy carbonyl group is pointing outward to the nearest oxygen network of the host (type II). In the refinement of the parameters, the occupancies of the 2 kinds of R6G molecules and the position of the non-center R6G molecule were varied.

The refinement was conducted using a non-linear least-squares program developed on the basis of Marquardt's algorithm (Bevington 1969). The Fourier syntheses were done using modified RSSFR-5 (Sakurai 1967). A 2-dimensional electron density map was also obtained by using the Maximum Entropy method (Sakata and Takata 1992). During the refinement, the isotropic temperature factors (B_{iso}) of the TN portion were fixed to 2.00 Å^2. For C, N, O atoms of the R6G portion, B = 10.0 Å^2 was used, according to Reynolds (1965). The incorporated 2.6-mol water was placed at 2.7 Å from the surface oxygen layer of the TN portion and its positional parameters were varied. Its position was derived from X-ray analysis of LiTN, which is consistent with the length of O-H··O hydrogen bonding.

RESULTS

Basal spacings of the R6G-TN complexes were constant at 21.7 to 22.2 Å for various R6G/TN ratios. Figure 4 presents typical XRD patterns of the product obtained at 105–110 °C. These patterns are depicted in the order (top to bottom) of descending R6G content of the specimen, with specific contents corresponding to those listed in Table 1. The lower-angle subpeak of 002 in specimen 4946 is a 001 peak of unreacted LiTN [d(001) = 12.3 Å]. The ratio of unreacted LiTN to R6G-TN complex was estimated as 0.27 by deconvolution of the 002 peak. As seen in the figure, the specimens oriented with their *ab* plane parallel to the holder surface. The 22-Å complex has a wide stability range, as the initial R6G-to-TN ratio varied from 0.08 to 8.0 by weight. The degree of intercalation was judged by the number of basal reflections and the peak width. At the optimum condition, the number of 001 reflections increased to 12, and full width half maximum (FWHM) of 001 was 0.2° in 2θ. Similar XRD patterns with d(001) of 22 Å were observed in the Ox4-TN complexes, which were synthesized at 120 °C under the autogenous pressure of that temperature.

The IR absorption of several bands decreased in intensity with increasing θ (Figure 5). Those at 1517, 1537 and 1621 cm^{-1} were assigned as the xanthene ring vibration. Similar dependence on θ was observed in the IR spectrum of Ox4-TN complex.

Figure 6 shows the typical DTA-TG patterns of the 22-Å composite. Two exothermal peaks at approximately 345 °C and 800–900 °C characterize the pattern, and the weight loss events correspond well to these peaks. The 345-°C peak was ascribed to the decomposition of R6G and the 800–900-°C peak to the oxidation of fragments formed from R6G.

https://doi.org/10.1346/CCMN.1997.0450109 Published online by Cambridge University Press

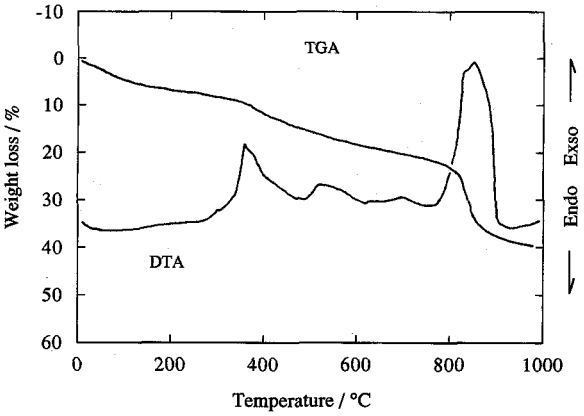

Figure 6. DTA-TG curves of the 22-Å composite (specimen 5120).

Several typical data of thermal and carbon analyses are summarized in Table 1 together with basal spacings. Weight loss was measured at 1000 °C by TG, and R6G content was determined by carbon analyses. Water content was calculated by assuming that the loss of R6G cation from the gallery was in the form of $R6G^{+} + \frac{1}{2}O^{-}$, and that the rest of the weight loss was due to the escape of water. Under this assumption, weight loss up to 200 °C was attributed to water loss, and loss at higher temperature was assigned to R6G and accompanying oxygen from the host layer. In the calculation for specimen 4946, the coexisting LiTN is assumed to have the same amount of water in its gallery as the reference LiTN. The Li content is that of unexchanged Li in the gallery, calculated by assuming one-to-one exchange of Li by R6G.

The *R*-factors obtained for each model are shown in Table 2, indicating the lowest *R*-factor in the case of the vertical model. The intensities (I_o) and observed structure factors (F_o) are listed together with the calculated *F*'s (F_c) for the vertical model ($R = 0.013$) in Table 3. The positional parameters and occupancies corresponding to the vertical model are also shown in Table 4. Here, error values in parentheses without a decimal point correspond to the least significant digit in the function values.

Table 1. Composition of the R6G-taeniolite composite.

Specimen	Weight loss (wt%)	R6G content (wt%)	Li content (wt%)	H_2O content (wt%)	R6G/TN (mole ratio)	Basal spacing (Å)
(LiTN)	16.5	0	1.6	16.5	0.0	12.27
4946	20	6	1.5	14.8	0.086	21.79
						12.3
4212	31	17	1.3	13.7	0.22	21.73
5638	34.5	26	1.2	8.0	0.33	21.81
5120	40	33	1.1	6.4	0.46	21.89

Table 2. Reliability factors for the 3 structure models.

	Parallel models		Vertical model
	Type I†	Type II‡	
R-factor	0.195	0.218	0.012

† Ethoxy carbonyl group is directed outwards.
‡ Ethoxy carbonyl group is directed inwards.

DISCUSSION

Taking the R6G size (Figure 7) into account, 2 possibilities for the orientation of R6G in the gallery of the taeniolite layer were considered to fit R6G in the 22-Å taeniolite frame: 1) three R6G arranged between the host layer with their xanthene rings parallel to the *ab* plane of the TN (parallel model); or 2) the longest axis of xanthene normal to the *ab* plane of the host; i.e., N atoms on the both sides of xanthene ring located near the sandwiching host layers, above and below (vertical model). As already described, both models were considered for refinement of the parameters.

In the present study, the vertical model is supported by the following evidence: 1) With the assumption that the R6G molecule is a rectangle (cross sections of 74 and 139 Å^2 for vertical and parallel models, Figure 7), the calculated areal ratios of R6G/TN range from 0.50 to 2.70 for the parallel model, and from 0.27 to 1.44 for the vertical one, as the R6G to TN ratio varies from 0.086 to 0.46 (Table 1). In the calculation, lattice parameters *a* and *b* of K-taeniolite (Toraya et al. 1977) were assumed for those of LiTN. In the case of the parallel arrangement, a change from single- to double-layered intercalation is inevitable; alternatively, the vertical model allows a single-layered state for the whole range of R6G content. Thus, the vertical model is compatible with the constant basal spacings for various R6G contents. 2) As listed in Table 2, the *R*-factor for the vertical model converged to the excellent value of 1.2%; on the other hand, as much as 20% was obtained for both parallel models (type I and type II). Figure 8 shows the result of Fourier and difference-Fourier syntheses together with the proposed vertical

Table 3. Intensities and observed and calculated structure factors for the vertical model of rhodamine–taeniolite complex.

hkl	I_0	$\|F_o\|$	F_c
001	100	74.67	74.73
002	34.4	87.24	86.96
003	1.644	29.47	−28.13
004	2.86	51.33	−53.15
005	2.26	58.02	−56.75
006	3.46	86.94	86.76
007	5.44	129.08	128.32
008	1.22	70.65	71.93
009	1.20	79.89	−81.16
00·10	1.15	88.80	−88.24

https://doi.org/10.1346/CCMN.1997.0450109 Published online by Cambridge University Press

Table 4. Positional parameters of R6G-taeniolite complex refined by using the vertical model.

Atomic positions (Å)	Atoms	
0	1 Li, 2 Mg	
0.932(7)†	2 F	
1.490(8)	4 O	
2.804(6)	4 Si	
3.544(9)	6 O	
5.74(2)	2.4 H_2O	
6.144	1.1 (CH_3, NH, CH_2)	0.55(1) R6G
7.344	1.1 (CH_3, C, C)	
8.32(2)	1.1 (0.5(O, O-CH_2-CH_3))	
8.544	1.1 (CH, CH)	
9.744	1.1 (C, C, 0.5C)	
10.07(2)	1.1 (C, CH)	
10.944	1.1 (0.5(O, C, C, CH))	

† Estimated errors indicate the parameters varied during the refinement. Thermal parameter 2.0 Å^2 was used for the atoms of taeniolite frame, and 10.0 Å^2 for those of R6G and H_2O.

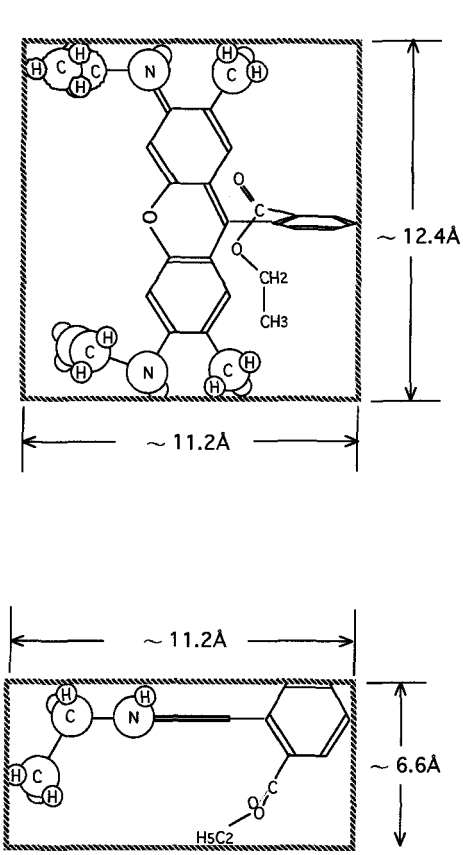

Figure 7. The configuration of rhodamine 6G in the gallery of a taeniolite: 1) a vertical view with respect to the xanthene ring; 2) a projection along the longest axis of the xanthene ring.

model of R6G. No significant residual electron densities were observed in the difference-Fourier map in the case of the vertical model. The obtained positional parameters of the atoms in the mica portion are compatible with those of TN refined by the single crystal X-ray method (Toraya et al. 1977). For the specimen whose data were submitted to least-squares refinement, TG-DTA and carbon analysis data indicate the mole ratio of TN to R6G is 0.45 to 1.00. This composition is consistent with the ratio R6G/TN = 0.55 (in mol) calculated from the occupancy of R6G in the gallery. 3) The IR absorption bands of 1331, 1517, 1537 and 1621 cm^{-1} showed the pleochroism expected for vertical orientation (it does not specify the rotation angle of the R6G; the xanthene plane has freedom of rotation in the vertical plane perpendicular to the *ab* plane) of the xanthene ring to the *ab* plane. Three of the 5 absorption bands are assigned to the in-plane xanthene ring vibration (1517, 1537 and 1621 cm^{-1}), and the 1331 cm^{-1} bands to the aromatic secondary amine, AR-NHR stretching. As for the 1621 cm^{-1} band, a contribution from N-H in-plane bending and deformation modes is also possible. The absorption of these bands reached a maximum at the polarization angle $\theta = 0°$, and decreased with the increase of θ to 90° for both the R6G- and Ox4-TN complexes. If the R6G orientation is parallel to the *ab* plane, pleochroism of these modes should be minimal.

To estimate the dimension of R6G in the complex, the configuration as depicted in Figure 7 was estimated, where the ethyl group attached to the nitrogen is directed into the R6G molecule, exposing the N atoms to the outer environment. This configuration results in the length of 12.4 Å, which is consistent with that between silicate layers in the 22-Å complex (Figure 8). It also allows direct contact between positively charged nitrogen and the negatively charged silicate surface, leading to a strong coulombic force which stabilizes the vertical orientation. The layer spacing in the 22-Å complex would correspond to 3 layers of R6G in the parallel orientation; however, the formation of R6G trimer has not been observed so far (Lopez Arbeloa et al. 1982).

R6G-clay complexes with 21-Å basal spacing have been reported for other clays such as montmorillonite (21.0 Å) and Laponite XLG (21.3 Å) (Grauer et al. 1984). Judging from the basal spacings, those compounds possibly have a vertical orientation, but their stability range expressed by the molal ratio of the (organic molecules)/(host silicates) are narrower than in the present study. In these cases, the basal spacings of these complexes were found to change gradually from 14 to 21 Å, according to the concentration increase of the intercalant in the complex. The enhanced stability of the vertical arrangement in the case of TN may be because the negative charge of the silicate layer of TN is larger than that of other hosts. The CEC of the present host, Li-fluor TN, is 157 ± 9 meq/100 g; on the

https://doi.org/10.1346/CCMN.1997.0450109 Published online by Cambridge University Press

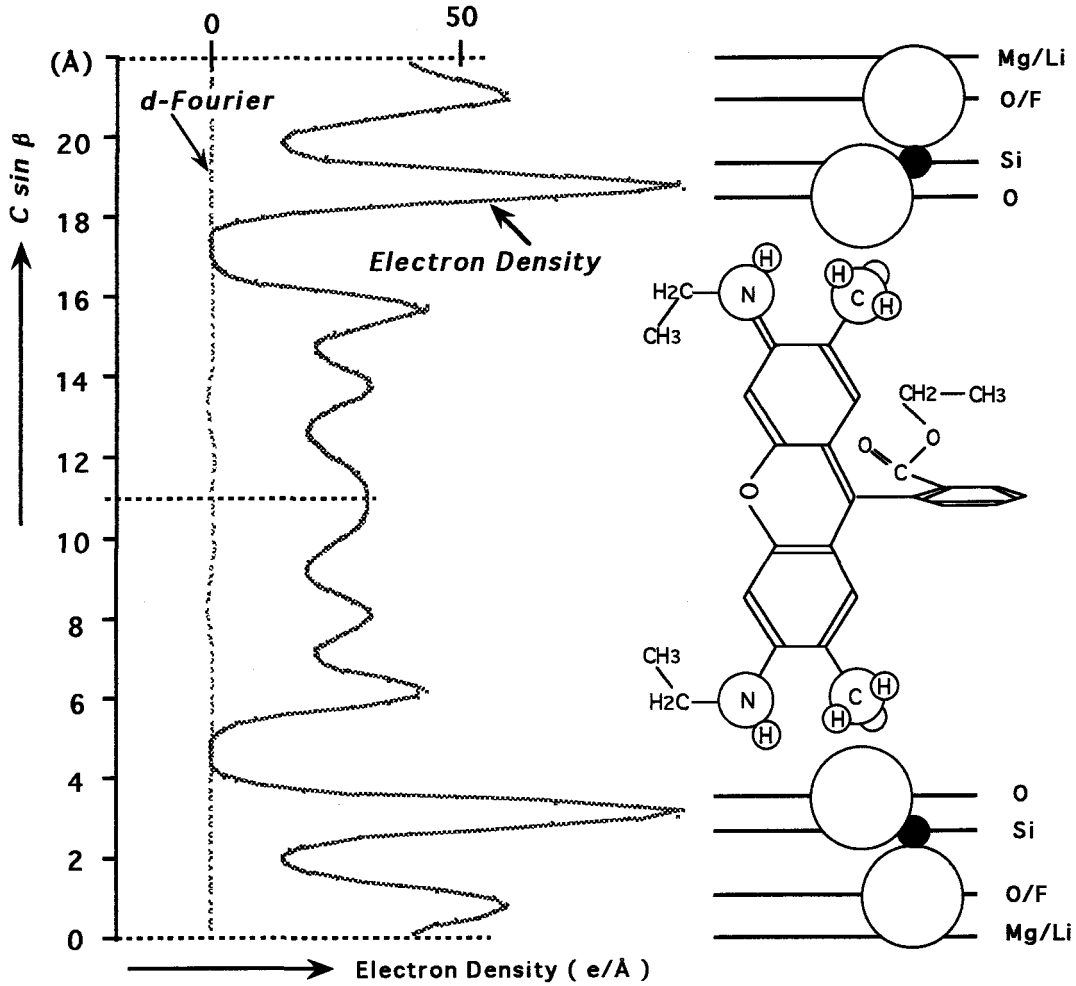

Figure 8. The orientation of rhodamine 6G derived by Fourier analyses.

other hand, those for hosts used in related studies were as low as 71–115 meq/100 g (Endo et al. 1986, 1988; Tapia Estevez et al. 1994; McBride 1985). High CEC would be expected to influence the orientation of R6G through the stronger coulombic force between host and guest.

The purpose of complexing R6G with TN was originally to increase the heat resistance of R6G. The exothermal peak at 370 °C (Figure 6) corresponds to that of a 345-°C signal for R6G measurement; consequently, the thermal stability of R6G in the complex was improved by 25 °C when compared with that of R6G itself. The large peak at 800–900 °C, which is not observed in LiTN, is due to the oxidization of the decomposed fragments of R6G.

CONCLUSION

R6G intercalation by ion exchange reaction to Li-fluor TN, with a high CEC of 157 ± 9 meq/100 g, yielded a complex of 22-Å basal spacing. The orientation of R6G was concluded to be perpendicular to the *ab* plane of the host. The stability range of the complex is, at least, from 0.06 to 0.46 (molar ratio of R6G to TN) which is wider than those so far reported for R6G-clay complexes having similar basal spacings. The stability of the vertical orientation may be due to a large coulombic force between the highly charged host layer and the positively charged N atoms that are bonded to both sides of the xanthene ring.

The thermal resistance of R6G was increased by 25 °C when intercalated in TN.

ACKNOWLEDGMENTS

The authors express their great appreciation to Dr. H. Nakazawa of the National Institute for Research in Inorganic Materials for his encouragement and advice for this work, and to Dr. J. R. Hester for his improvement of the English.

REFERENCES

Bevington PR. 1969. Data reduction and error analysis for the physical sciences. NY: McGraw-Hill. 336 p.

Cenens J, Vliers DP, Schoonheydt RA, DeSchryer FC. 1987. Spectroscopic study of the surface chemistry of proflavine

https://doi.org/10.1346/CCMN.1997.0450109 Published online by Cambridge University Press

on clay minerals. In: Schultz LG, van Olphen H, Mumpton FA, editors. Proc International Clay Conference; 1985; Denver. Bloomington, IN: Clay Miner Soc. p 352–538.

DellaGuardla RA, Thomas JK. 1983. Photoprocesses on colloidal clay systems. Tris(2,2′-bipyridine) ruthenium(II) bound to colloidal kaolin and montmorillonite. J Phys Chem 87:990–998.

Endo T, Nakada N, Sato T, Shimada M. 1988. Fluorescence of the clay-intercalated xanthene dyes. J Phys Chem Solids 49:1423–1428.

Endo T, Nakada N, Sato T, Shimada M. 1989. The fluorescence properties of coumarine dye intercalated in a swelling clay. J Phys Chem Solids 50:133–137.

Endo T, Sato T, Shimada M. 1986. Fluorescence properties of the dye-intercalated smectite. J Phys Chem Solids 47: 799–804.

Fukushima Y, Inagaki S. 1987. Synthesis of an intercalated compound of montmorillonite and 6-polyamide. J Incl Phenomenon 5:473–482.

Grauer Z, Avnir D, Yariv S. 1984. Adsorption characteristics of rhodamine 6G on montmorillonite and laponite, elucidated from electronic absorption and emission spectra. Can J Chem 62:1889–1894.

Ibers JA, Hamilton WC. 1974. International tables for X-ray crystallography, vol 4. Birmingham: Kynoch Pr. 366 p.

Lopez Arbeloa F, Llona Gonzalez I, Ruiz Ojeda P, Lopez Arbeloa I. 1982. Aggregate formation of rhodamine 6G in aqueous solution. J Chem Soc, Faraday Trans 78:989–994.

Margulies LH, Rozen H, Cohen E. 1985. Energy transfer at the surface of clays and protection of pesticides from photodegradation. Nature 315:658–659.

McBride MB. 1985. Surface reactions of 3,3′,5,5′-tetramethyl benzidine on hectorite. Clays Clay Miner 33:510–516.

Nijs H, Fripiat JJ, Van Damme H. 1983. Visible-light-induced cleavage of water in colloidal clay suspensions: A new example of oscillatory reaction at interfaces. J Phys Chem 87:1279–1282.

Okada A, Kawasumi M, Usuki A, Kojima Y, Kurauchi T, Kamigaito O. 1990. Nylon 6-clay hybrid. Mater Res Soc Symp Proc 171:45–50.

Reynolds RC Jr. 1965. An X-ray study of an ethylene glycol-montmorillonite complex. Am Mineral 50:990–1001.

Sakata M, Takata M. 1992. Electron density distribution from powder diffraction experiment. Nippon Kesshou Gakkaishi 34:100–109.

Sakurai T. 1967. Universal crystallographic computation program system (II). Tokyo: Cryst Soc Jpn. 270 p.

Schollenberger CJ, Simon RN. 1946. Determination of exchange capacity and exchangeable bases in soil—Ammonium acetate method. Soil Sci 59:13–24.

Tapia Estevez MJ, Lopez Arbeloa F, Lopez Arbeloa T, Lopez Arbeloa I, Schoonheydt RA. 1994. Spectroscopic study of the adsorption of rhodamine 6G on Laponite B for low loadings. Clay Miner 29:105–113.

Toraya H, Iwai S, Marumo F. 1977. The crystal structure of taeniolite, $KLiMg_2Si_4O_{10}F_2$. Z Kristallogr 146:73–83.

Villemure G, Detellier C, Szabo AG. 1986. Fluorescence of clay-intercalated methylviologen. J Am Chem Soc 108: 4658–4659.

Wang MS, Pinnavaia TJ. 1994. Clay-polymer nanocomposites formed from acidic derivatives of montmorillonite and an epoxy resin. Chem Mater 5:468–474.

Wu J, Lerner MM. 1993. Structural, thermal and electrical characterization of layered nanocomposites derived from Na-montmorillonite and polyethers. Chem Mater 6:835–838.

Yamada H, Fujita T, Nakazawa H. 1988. Design and calibration of a rapid quench hydrothermal apparatus. Seramikkusu Ronbunshi 96:1041–1044.

(Received 16 October 1995; accepted 13 April 1996; Ms. 2700)

https://doi.org/10.1346/CCMN.1997.0450109 Published online by Cambridge University Press